Interdecadal Changes in the Major Modes of Asian–Australian Monsoon Variability: Strengthening Relationship with ENSO since the Late 1970s*

BIN WANG+

Department of Meteorology, and International Pacific Research Center, University of Hawaii at Manoa, Honolulu, Hawaii

JING YANG

Department of Meteorology, and International Pacific Research Center, University of Hawaii at Manoa, Honolulu, Hawaii, and LASG, Institute of Atmospheric Physics, Chinese Academy of Sciences, Beijing, China

TIANJUN ZHOU AND BIN WANG

LASG, Institute of Atmospheric Physics, Chinese Academy of Sciences, Beijing, China

(Manuscript received 4 April 2007, in final form 12 July 2007)

ABSTRACT

The present paper develops an integral view of the year-to-year variability across the entire Asian–Australian monsoon (A–AM) system, which covers one-third of the global tropics between 40° and 160°E. Using season-reliant empirical orthogonal function (S-EOF) analysis, the authors identified two major modes of variability for the period 1956–2004. The first exhibits a prominent biennial tendency and concurs with the turnabout of El Niño–Southern Oscillation (ENSO), providing a new perspective of the seasonally evolving spatiotemporal structure for tropospheric biennial oscillation. The second mode leads ENSO by one year. The remote El Niño forcing, the monsoon–warm pool ocean interaction, and the influence of the annual cycle are three fundamental factors for understanding the behavior of the first mode. The monsoon–ocean interaction is characterized by a positive feedback between the off-equatorial convectively coupled Rossby waves and the underlying sea surface temperature (SST) "dipole" anomalies.

Since the late 1970s the overall coupling between the A–AM system and ENSO has become strengthened. The relationships between ENSO and the western North Pacific, East Asian, and Indonesian monsoons have all become enhanced during ENSO's developing, mature, and decaying phases, overriding the weakening of the Indian monsoon–ENSO anticorrelation during the developing phase. Prior to the late 1970s (1956–79), the first mode shows a strong biennial tendency, and the second mode does not lead ENSO. After 1980, the first mode shows a weakening biennial tendency, and the second mode provides a strong precursory signal for ENSO. These interdecadal changes are attributed to increased magnitude and periodicity of ENSO and the strengthened monsoon–ocean interaction.

1. Introduction

A great portion of the monsoon literature has studied the year-to-year variability in *various monsoon regions* in the Eastern Hemisphere, including the Indian monsoon (e.g., Mooley and Parthasarathy 1984; Shukla 1987), the Indonesian–Australian monsoon (e.g., Yasunari and Suppiah 1988; Hamada et al. 2002), the East Asian (EA) monsoon (e.g., Nitta 1987; Huang and Wu 1989; Zhou and Yu 2005), the western North Pacific (WNP) monsoon (Wu and Wang 2000), and the eastern African monsoon (e.g., Janowiak 1988; Okoola 1999). The rainfall and circulation anomalies in many of the aforementioned regions exhibit a major 2- to 3-yr spectral peak (e.g., Meehl 1987; Lau and Shen 1988; Ropelewski et al. 1992; Chen and Yoon 2000; Meehl and Arblaster 2002). Comprehensive reviews have been recently provided by Webster (2006) and Yang and Lau (2006).

* International Pacific Research Center Publication Number 510 and School of Ocean and Earth Science and Technology Publication Number 7314.

+ Current affiliations: LASG, Institute of Atmospheric Physics, Chinese Academy of Sciences, Beijing, and College of Marine Environment, Ocean University of China, Qingdao, China.

Corresponding author address: Prof. Bin Wang, Department of Meteorology, and IPRC, University of Hawaii at Manoa, 2525 Correa Rd., Honolulu, HI 96822.
E-mail: wangbin@hawaii.edu

DOI: 10.1175/2007JCLI1981.1

© 2008 American Meteorological Society

The Asian–Australian monsoon (A–AM) region, spanning from 30°S to 40°N and from about 40° to 160°E, covers one-third of the global tropics and subtropics. The entire Indo-Pacific warm pool is under the influence of the A–AM. Efforts have been made toward understanding the A–AM's broad-scale interannual variability (e.g., Meehl 1987; Webster and Yang 1992; Navarra et al. 1999; Kim and Lau 2001; Wang et al. 2003; Lau and Wang 2005). These studies have paid specific attention to the relationship between El Niño–Southern Oscillation (ENSO) and the monsoon. Since the late 1970s, an interdecadal climate regime "shift" has occurred in the North Pacific SST and sea level pressure fields (e.g., Nitta and Yamada 1989; Trenberth and Hurrell 1994; Graham 1994). Concomitantly, the inverse relationship between the Indian summer monsoon (ISM) rainfall and Niño-3.4 SST anomalies has broken down (e.g., Kumar et al. 1999). At the same time, a notable change between the East Asian monsoon and ENSO in northern China and Japan has emerged (Wu and Wang 2002), and the negative correlation between Indonesian monsoon rainfall and ENSO has become enhanced since the late 1970s (Chang et al. 2004). Now, it is necessary to develop an integral view of the variability across the entire A–AM system.

So, what are the major modes of interannual variability in the entire A–AM system? The answer to this question is not straightforward because the year-to-year variations in the vast A–AM domain exhibit remarkable regional differences and depend strongly on the seasonal march and evolution of ENSO. When conventional empirical orthogonal function (EOF) analysis and singular value decomposition (SVD) analysis are applied to the seasonal mean precipitation anomalies in the A–AM region, the obtained first mode is governed by the anomalies associated with the ENSO mature phase, which primarily reflects the Indonesian–Australian summer monsoon variability but not the Asian summer monsoon variations (e.g., Lau and Wu 2001). To delineate the variability of the Asian summer monsoon, an EOF analysis has been applied to the boreal summer season only. The resultant first mode is dominated by the monsoon anomalies during the developing summer of an ENSO warm event (e.g., Webster and Yang 1992). However, recent studies have indicated that the largest rainfall variability occurs in boreal fall over East Africa, the equatorial eastern Indian Ocean, the Maritime Continent, and the southern Indian Ocean in association with the Indian Ocean dipole (IOD) mode or zonal mode (Saji et al. 1999; Webster et al. 1999). Further, major summer rainfall anomalies over East Asia often occur in the summer of ENSO decaying years (e.g., Huang and Wu 1989). Thus, it is important to appreciate that the interannual variability in the immense A–AM region is highly season dependent and varies remarkably by region; thus, conventional EOF or SVD methods are not the best way to properly describe the principal modes of the A–AM system. In the present paper, we will use a modified version of EOF analysis to extract the major modes of variability.

Three fundamental questions that motivated the present study are as follows: 1) What are the major modes of interannual variability in the entire A–AM system? 2) Is there any interdecadal change in these modes? 3) Which processes give rise to the first mode of variability and its interdecadal variation? Addressing these questions is imperative for understanding the physical processes that govern A–AM variability. The results also provide an objective validation of the atmospheric general circulation model (GCM) and the coupled atmosphere–ocean GCMs in their climate simulations and seasonal predictions of A–AM variations.

Section 2 briefly describes the methodology and datasets used in the present study. Section 3 articulates the major modes of the A–AM interannual variability. Section 4 further examines whether these major modes have experienced decadal-to-interdecadal variations over the past half century. Section 5 discusses the possible processes that give rise to the first mode and its interdecadal change. Last, the final section summarizes the study and its findings.

2. Season-reliant EOF analysis and datasets

To depict season- and region-dependent anomalies and their intrinsic linkages in the year-to-year variability of the A–AM system as a whole, we applied a newly proposed method called season-reliant EOF (S-EOF) analysis (Wang and An 2005). The purpose of S-EOF is to depict seasonally evolving anomalies throughout a full calendar year. For this analysis, we adopted the concept of "monsoon year" (Meehl 1987; Yasunari 1991), which spans from the summer of year 0, referred to as June–August(0) [JJA(0)], to the spring of the following year (year 1) called March–May(1) [MAM(1)]. For this purpose, a covariance matrix was constructed using four consecutive seasonal mean anomalies for each year; in other words, we treated the anomalies for JJA(0), September–November(0) [SON(0)], December–February(0/1) [DJF(0/1)], and MAM(1) as a "yearly block," labeled year 0, in which the sequence of anomalies commences. After the EOF decomposition was performed, the yearly block was then divided into four consecutive seasonal anomalies so that one obtains

a seasonally evolving pattern of monsoon anomalies in each monsoon year for each eigenvector.

We used the 850-hPa zonal wind as a primary variable for the analysis within the A–AM domain (25°S–35°N, 40°–160°E) because it is more reliable than a divergent circulation component and because the wind record provides a much longer analysis record than observed precipitation data, such as those from the Climate Prediction Center (CPC) Merged Analysis of Precipitation (CMAP). Such a long period of data is desirable for deriving dependable interannual variability patterns and is indispensable for examining interdecadal variation.

The data used in the present study consist of 1) the National Centers for Environmental Prediction–National Center for Atmospheric Research (NCEP–NCAR) reanalysis data from 1956 to 2004, which is a dataset generated from a "frozen" version of the NCEP medium-range forecast model and its operational spectral statistics interpolation procedure (Kalnay et al. 1996); 2) the 40-yr European Centre for Medium-Range Weather Forecasts Re-Analysis (ERA-40) dataset from 1958 to 2001 (Uppala et al. 2005), which involves comprehensive use of satellite observations; 3) the sea surface temperature (SST) data from the NOAA Extended Reconstructed Sea Surface Temperature version 2 (Smith and Reynolds 2004); and 4) the precipitation reconstruction data over land (PREC/L") compiled for the period of 1948–2004 by the Climate Prediction Center at the National Centers for Environmental Prediction (Chen et al. 2002).

To focus on interannual variation, a Fourier harmonic analysis was applied to the time series of seasonal mean anomalies. The harmonics with periods longer than 8 yr were removed from the anomalous time series: thus, the filtered data describe interannual variations. Extensive sensitivity experiments have been done with different combinations of variables and datasets, and it was found that the large-scale interannual variations derived from the two reanalysis datasets for their common period of 1958–2001 are highly consistent, adding fidelity to the robustness of the results. For brevity, we will present only the results derived from NCEP–NCAR reanalysis.

3. Two major modes of interannual variability (1956–2004)

Figure 1 shows the eigenvalues of the first five S-EOF modes in the 850-hPa zonal winds derived for the period of 1956–2004. The first two modes account for, respectively, 25.2% and 10.1% of the total variance.

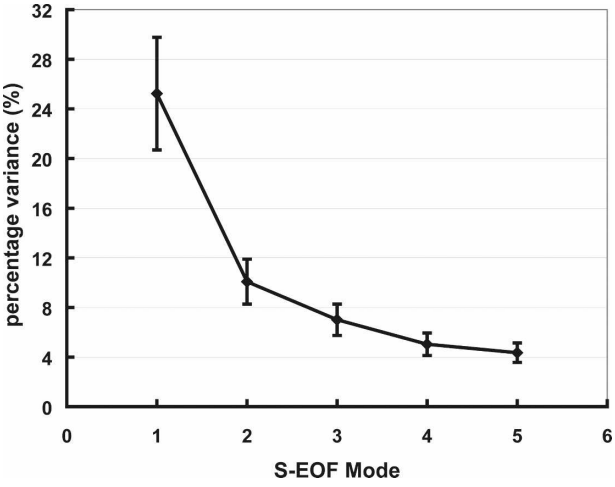

FIG. 1. Percentage variance (%) explained by the first five season-reliant EOF modes of the 850-hPa zonal winds. The bars represent one standard deviation of the sampling errors.

Applying the criterion proposed by North et al. (1982), we found that the first two modes are well distinguished from each other and from the rest modes at the 95% confidence level. These two modes are considered statistically distinguishable and significant. We have confined our analysis to these two major modes.

a. The first (leading) mode

Figure 2 presents the time series of the first principal component (Fig. 2a) along with its power spectrum (Fig. 2b). The principal component (PC1) has double spectral peaks at 2.5 and 5 yr. The 2.5-yr peak is more significant than the 5-yr peak. Note that in the S-EOF analysis, no SST information was involved. However, PC1 closely links to the eastern Pacific SST variations (Table 1). The simultaneous correlation coefficient between PC1 and the ENSO index, the Niño-3.4 SST anomaly, reaches 0.83, indicating that the seasonally evolving patterns of the first mode concur with ENSO's turnabout from a warming to a cooling phase. For the first mode, year 0 represents the developing year of El Niño, while year 1 implies a decaying year of El Niño.

Figure 3 shows the seasonally evolving spatial patterns (eigenvectors) of the first mode. Note that the eigenvector was derived by using only the 850-hPa wind anomalies. The 850-hPa meridional wind anomalies, the 500-hPa vertical pressure velocity anomalies, and precipitation anomalies were obtained using regression of the corresponding fields with reference to the first principal component. The anomalies in JJA(1) were also regressed against the first principal component at a 1-yr lag. If one performs a multivariate S-EOF of 850-hPa zonal and meridional winds, 500-hPa vertical pres-

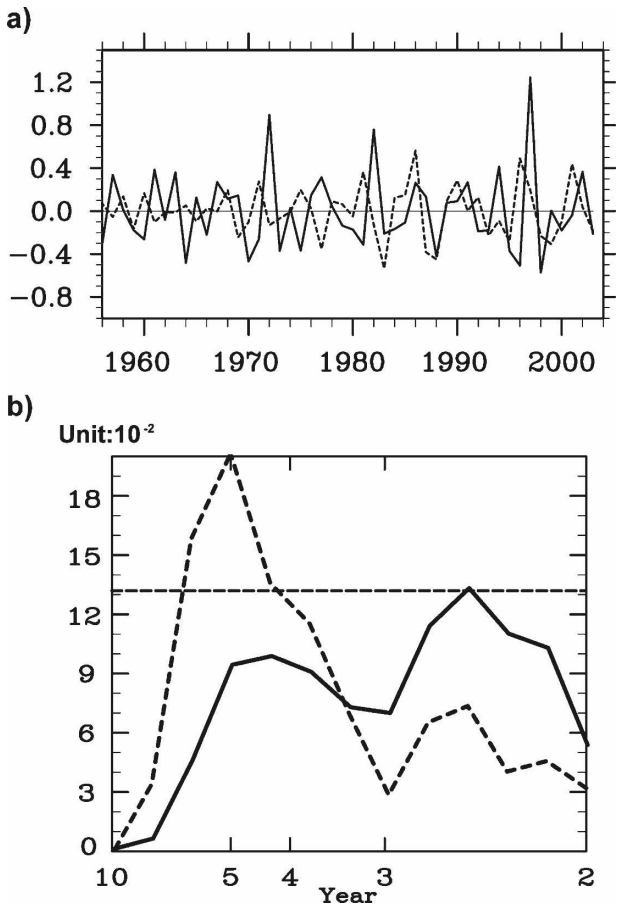

FIG. 2. (a) Time series and (b) their corresponding power spectra of the first (solid) and second (dashed) principal components. The horizontal thin dashed line in (b) denotes white noise power density. A spectrum with a peak above the horizontal thin dashed line implies that it is distinguished from a white noise spectrum with a confidence level over 95%.

sure velocity, and precipitation anomalies, the resultant patterns highly resemble those shown in Fig. 3.

The first notable feature in Fig. 3 is the reversal of the monsoon anomalies from the first summer to the next. The anomalies in JJA(0) are characterized by descent over the Maritime Continent and ascent over the Philippine Sea, an associated anomalous anticyclone (AC) ridge extending from the Maritime Continent to the Arabian Sea, and an anomalous cyclone over the western North Pacific along 20°N. In the A–AM central region (between 20°S and 30°N), the anomalous 850-hPa winds and 500-hPa vertical motion are nearly mirror images when comparing the first summer, JJA(0), and the next summer, JJA(1).

The second prominent feature is that the seasonally evolving anomalies are characterized by two prominent off-equatorial anticyclonic anomalies, the south Indian Ocean (SIO) and the western North Pacific (WNP) anticyclones, which alternately dominate the monsoon anomalies over the Indian Ocean sector in year 0 and the western Pacific sector in year 1. To quantify the strength of the tropical SIO and WNP anticyclones, we computed the anticyclonic vorticity anomalies for SIO in the region 5°–20°S, 60°–100°E and for the tropical WNP in the region 5°–20°N, 120°–160°E. These two regions are shown in the SON(0) and MAM(1) panels in Fig. 3a. The anomalous SIO anticyclone begins in JJA(0), develops rapidly, reaches its peak in SON(0), and then decays over the next two seasons (Fig. 4). The tropical WNP anomalous anticyclone begins near the northern Philippines in SON(0), rapidly develops in DJF(0/1), attains its peak during the following spring MAM(1), and then persists and extends eastward through the next summer (Fig. 4). The reason why the Philippine Sea anticyclone develops in the fall of the ENSO developing phase was discussed in detail by Wang and Zhang (2002). For brevity we will not repeat here. The evolution of these two anomalous anticyclones induces significant precipitation anomalies in various regions of the A–AM, as depicted by the color shading in Fig. 3b. The SIO anticyclone causes anomalous rainfall over the Maritime Continent, northern Australia, equatorial East Africa, South Africa, and Madagascar. On the other hand, the WNP anomalous anticyclone is responsible for precipitation anomalies over Southeast Asia, East Asia, and the WNP.

The third feature is the eastward shift of the monsoon circulation anomalies from the Indian Ocean to the western Pacific, which can best be seen by looking at the equatorial zonal wind anomalies (Fig. 5a). The eastward shift has also been presented through the propagation of the equatorial convective maxima involved in the tropospheric biennial oscillation (TBO) in the previous study of Meehl (1987). The diverging point between the equatorial westerly and easterly anomalies migrates systematically eastward along the equator from 100°E in JJA(0) to 160°E in MAM(1). The mi-

TABLE 1. Lead–lag correlation coefficients between the boreal winter Niño-3.4 SST anomalies (SSTA) and the principal components of the first and second S-EOF modes of the A–AM. The notation (0) denotes a reference year and (1) denotes the following year. The correlation coefficients that are statistically significant at 95% confidence level are in boldface.

	S-EOF1(0)	S-EOF2(0)
	56–04	56–04
Niño-3.4 SSTA(0)	**0.83**	0.13
Niño-3.4 SSTA(1)	−0.29	**0.73**

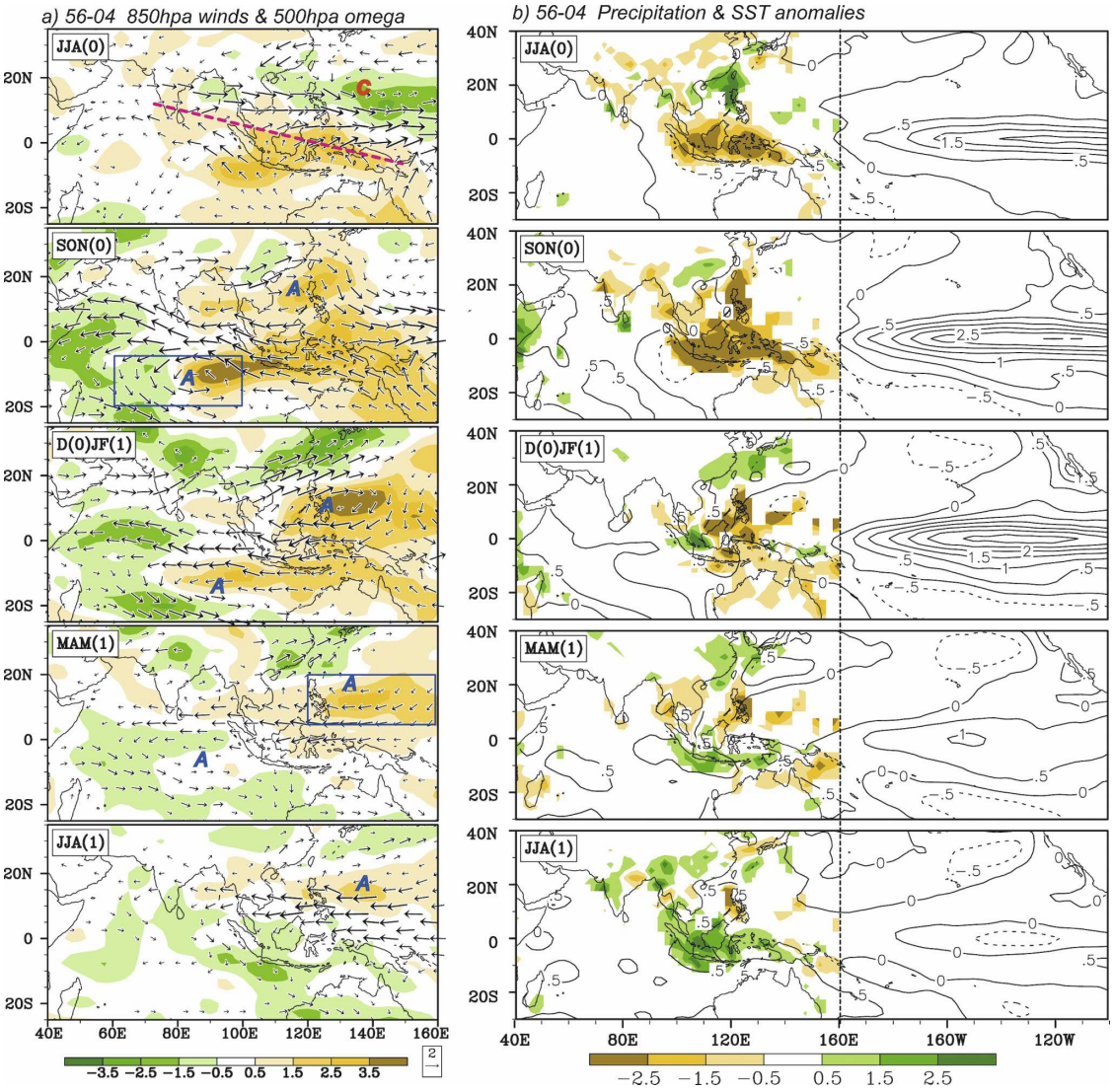

FIG. 3. (a) Seasonally evolving spatial patterns of the first leading S-EOF mode of the interannual variability of the Asian–Australian monsoon system including anomalous patterns of the 850-hPa zonal winds, regressed meridional winds (wind vectors, m s^{-1}), and regressed 500-hPa vertical (pressure) velocity anomalies (color shading, 10^{-2} hPa^{-1}). Only wind anomalies with speed exceeding 0.6 m s^{-1} are shown. (b) The corresponding seasonal mean precipitation anomalies over the continents and islands (color shading, mm day^{-1}) and SST anomalies (contours, K) that were regressed with respect to the first principal component. The rectangular regions in (a) denote the tropical south Indian Ocean and western North Pacific regions where the vorticities are calculated (see Fig. 4).

gration speed is about 7° longitude per month (or 0.27 m s^{-1}). The strongest easterly anomalies are observed during SON(0) over the eastern Indian Ocean, while the strongest westerly anomalies occur from JJA(0) to SON(0) in the western Pacific, which slightly leads the maximum easterly anomalies in the Indian Ocean.

The first mode accounts for about 25% of the total variance. But this fraction accounts for the percentage variance averaged in four consecutive seasons and over the entire A–AM domain (25°S–35°N, 40°–160°E). Note that the fractional variances vary by location and season (Fig. 6a). The largest fractional variance in 850-hPa zonal winds accounts for over 70% of the total variance in the equatorial western Pacific and the Indian Ocean. The largest fractional variance in 500-hPa vertical velocity (over 50%) is found over the Philippine Sea and Indonesia (figure not shown).

b. *The second mode*

The second principal component (PC2) exhibits a single spectral peak centered at 5 yr (Fig. 2b). The PC2 time series has a maximum correlation coefficient

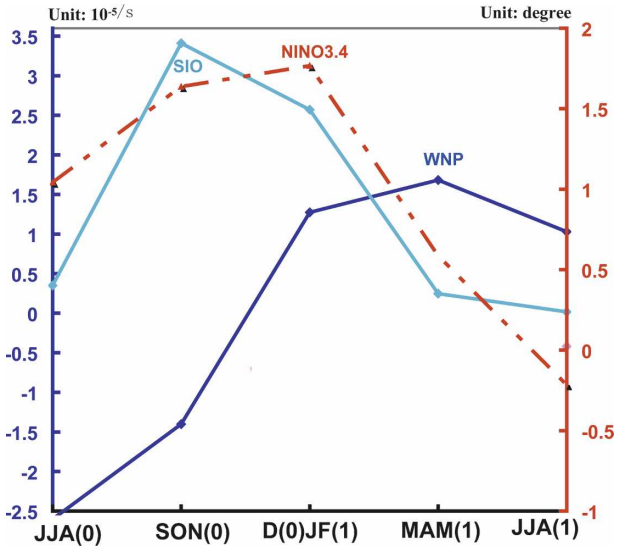

FIG. 4. Seasonal variations of the anomalous SIO anticyclonic vorticity averaged over the region 5°–20°S, 60°–100°E (Fig. 3a) and the anomalous WNP anticyclonic vorticity averaged over the region 5°–20°N, 120°–160°E (Fig. 3a), which are computed from Fig. 3. Shown also are the regressed Niño-3.4 SST anomalies with respect to the first principal component of the S-EOF mode.

(0.73) with the Niño-3.4 SST anomalies when PC2 leads Niño-3.4 by 1 yr (Table 1). This high correlation indicates that the second S-EOF mode leads ENSO by 1 yr, thus providing A–AM precursory conditions for ENSO.

Figure 7 presents the seasonally evolving spatial patterns of the second S-EOF mode. What are the major features of the anomalous A–AM one year prior to El Niño? We note that the wind anomalies in JJA(0) associated with the second S-EOF mode are nearly mirror images of those in JJA(1) of the first S-EOF mode. Since JJA(1) of the first mode represents a decaying El Niño, the JJA(0) pattern of the second S-EOF reflects the anomalies associated with a decaying La Niña. Therefore, in the summer prior to an El Niño developing year, the A–AM anomaly characterizes anomalous conditions that resemble those of a decaying La Niña episode. In SON(0), the SST in the tropical Pacific is nearly normal (shown by the contours in Fig. 7b) and the wind anomalies account for only a small fraction of the total variance (Fig. 6b). Both factors suggest that the coupled system is in a transitional phase. Of note is that the occurrence of the increased rainfall anomalies over the Maritime Continent during SON(0) leads to the warming occurring near the date line during DJF(0/1). Both signals are the earliest ancestors of El Niño.

The precursors become more evident in the following northern winter DJF(0/1), which is about 12 months prior to an El Niño peak. The western Pacific westerly anomalies rapidly intensify (Fig. 7a) and, at the same time, warming occurs near the date line (shown by the contours in Fig. 7b). The anomalous westerly that is north of New Guinea accounts for a substantial amount (30%–50%) of the total variance during the northern winter (Fig. 6b). Note also that reduced rainfall emerges over the western Maritime Continent (color shading in Fig. 7b). In the time between the northern winter and the ensuing spring, further simultaneous development occurs for the anomalous westerly in the equatorial Pacific, the suppressed rainfall over the Maritime Continent, and the warming in the central-eastern Pacific. By JJA(1), a well-developed El Niño is seen (Fig. 7b).

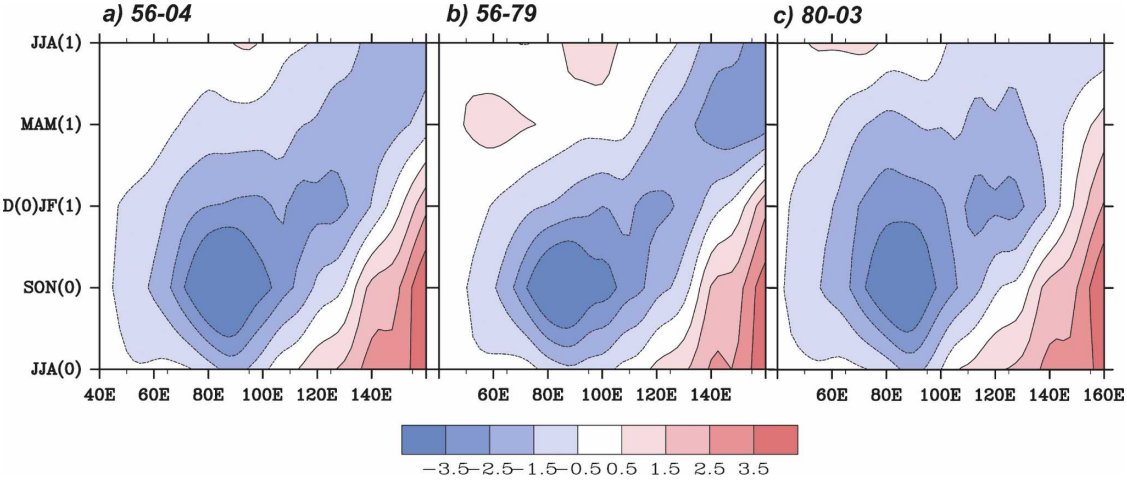

FIG. 5. Longitude–time diagram of the 850-hPa zonal wind averaged in the equatorial region between 5°S and 5°N for (a) 1956–2004, (b) 1956–79, and (c) 1980–2003. Winds (m s^{-1}) are computed from Fig. 3a for (a) and from Fig. 9a for (b) and (c).

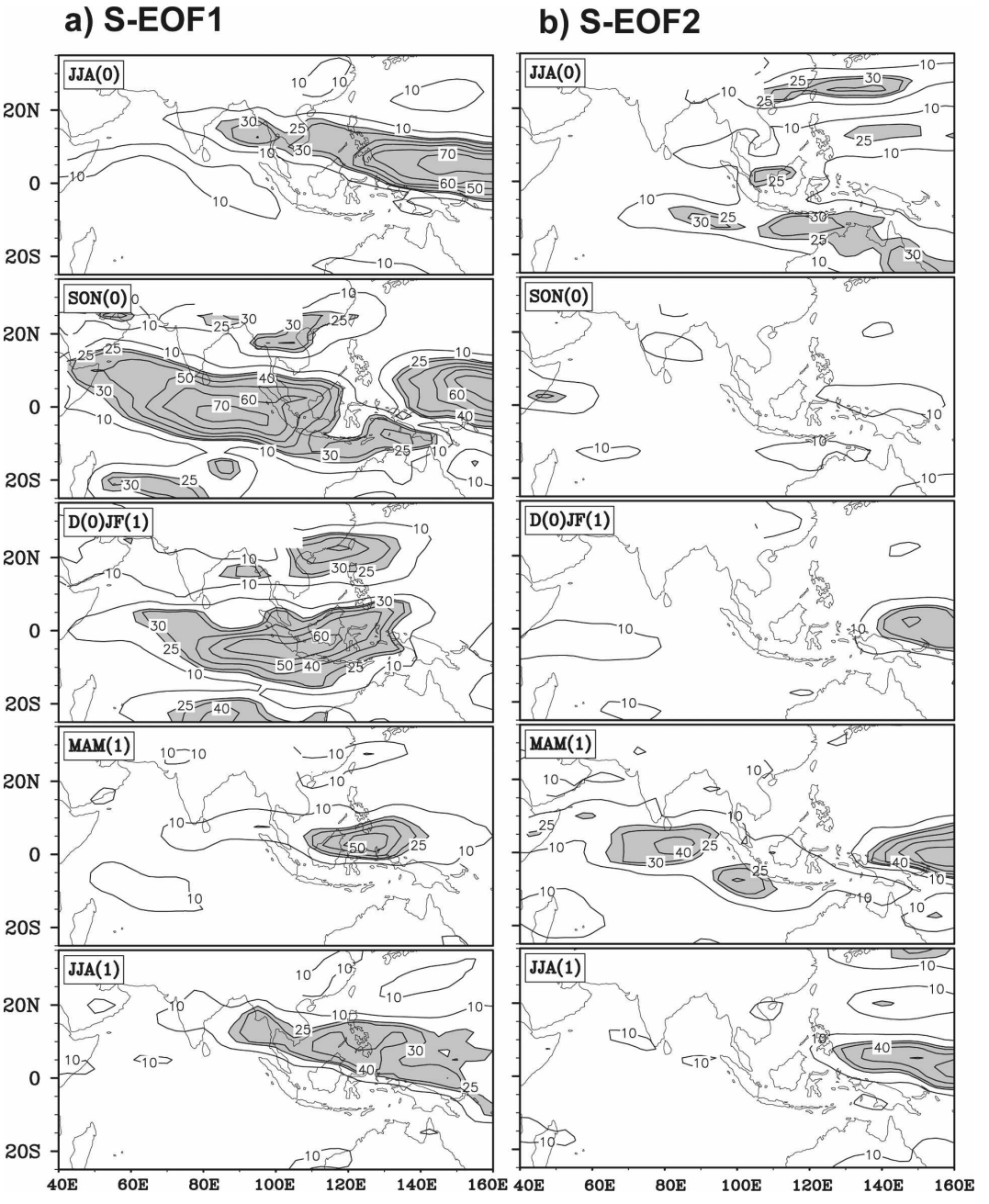

FIG. 6. (a) The percentage variance of the 850-hPa zonal wind accounted for by the first S-EOF mode. The shadings outline the regions of percentage variance higher than 25%. (b) As in (a) but for the second EOF-mode.

4. Interdecadal variation in the two leading modes of A–AM variability

Different from previous studies, which were focused on the regional monsoon–ENSO relationship, we examine the interdecadal change in the entire A–AM system in terms of the two major modes described in section 3. Here, so as to get same sample size for comparison, we contrast the major modes of A–AM interannual variations for two epochs: 1956–79 (pre-1979 or the first epoch) and 1980–2003 (post-1979 or the second epoch). The data used were derived from NCEP–NCAR reanalysis. Several sensitivity tests were made regarding the choice of dataset and the epochal periods. A parallel study has been carried out using ERA-40 reanalysis for two similar epochs: 1958–79 and 1980–2001. The results obtained from the two analyses are nearly the same (note that the analyses used an inter-

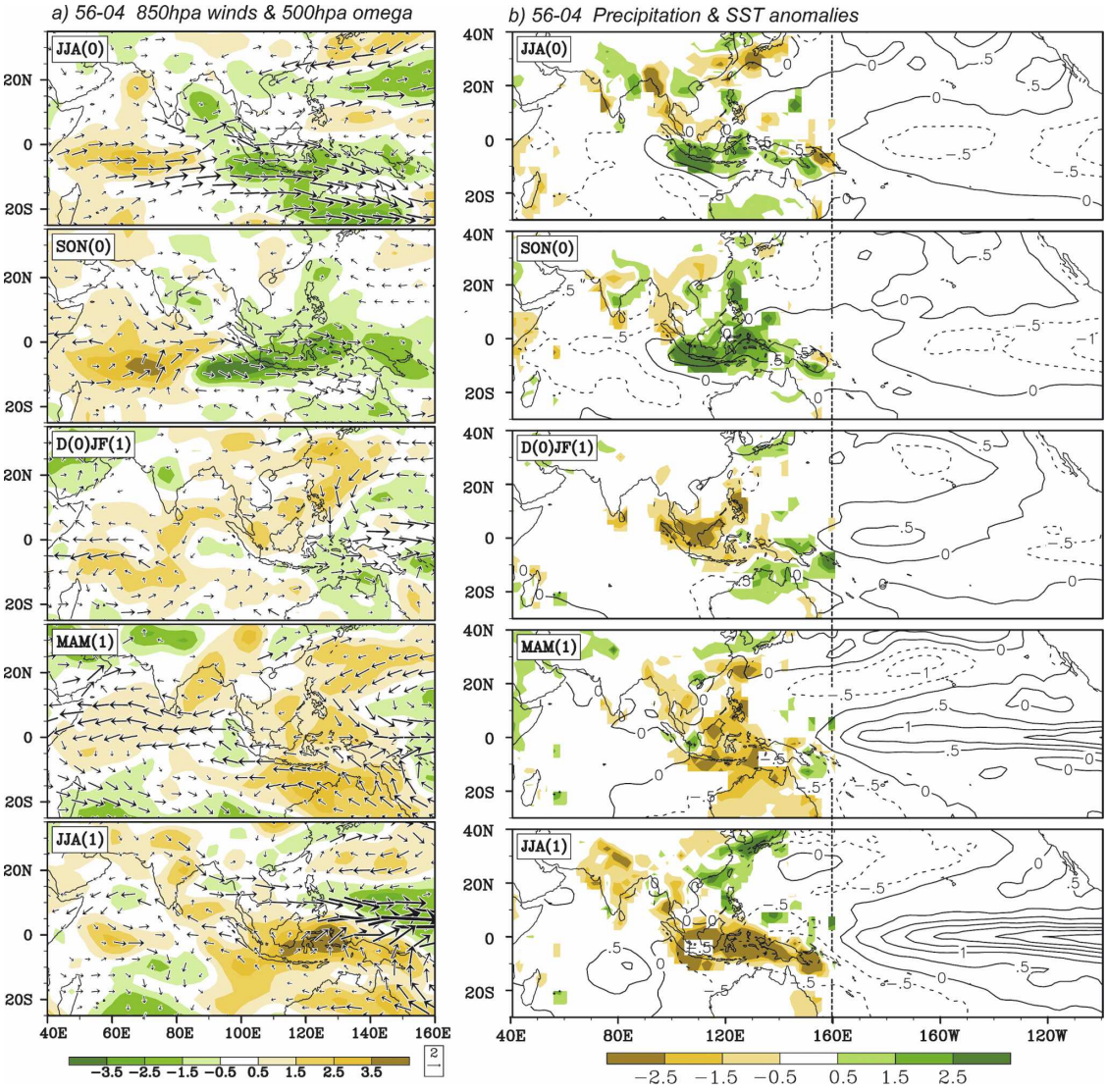

FIG. 7. As in Fig. 3a but for the second S-EOF mode.

annual component, which reflects variability in intervals of 2–8 yr only). Therefore, only NCEP–NCAR reanalysis data are presented in this section. In addition, we analyzed the results for alternative choices of epochs, such as 1956–76 and 1977–2004 using NCEP–NCAR reanalysis. The results are nearly the same as those shown in this section, suggesting that the interdecadal changes are robust as long as the two epochs are divided in the later half of the 1970s.

a. Changes in the first mode

The fractional variance accounted for by the first S-EOF mode has increased from 24.2% to 31.2% since the late 1970s. The quasi-biennial oscillation is more evident in the pre-1979 epoch (Fig. 8a), which is confirmed by a 2–3-yr spectral peak (figure not shown). In the post-1979 period, the biennial tendency is weaker and only associated with the turnabout from warming to cooling during the three major El Niño events (1982–83, 1994–95, and 1997–98; shown in Fig. 8a).

The relationship between the first leading mode and ENSO has shown subtle changes from the first epoch to the second. As shown in Table 2, for both epochs, the first PC and Niño-3.4 anomaly exhibits strong positive correlation, indicating that the first modes are associated with El Niño turnabout in both epochs. But, the association is stronger during the recent epoch, as indicated by the correlation coefficient's increase from 0.82 to 0.89. More significantly, only in the pre-1979 epoch, the first PC has a significant negative correlation

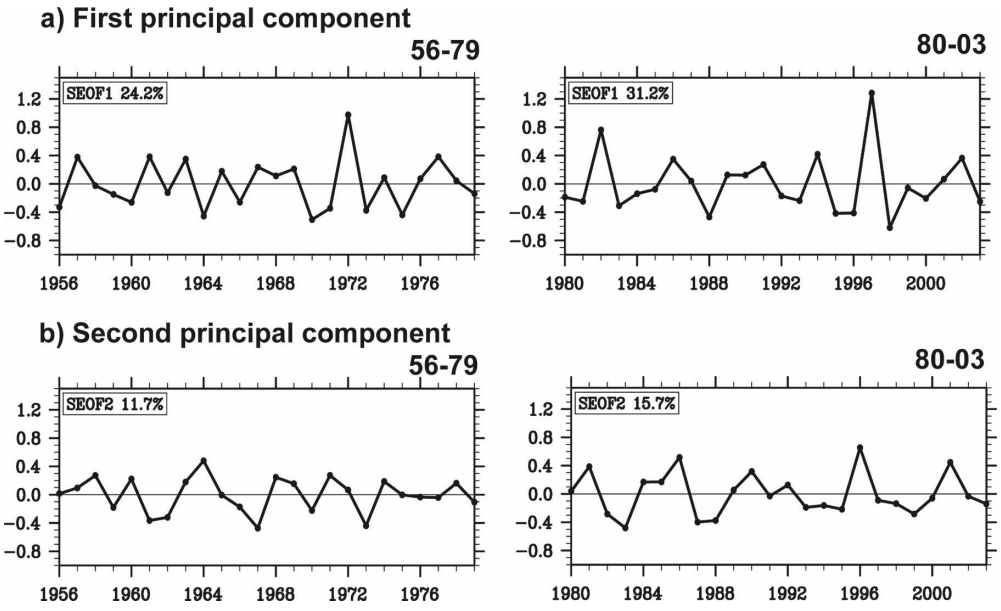

FIG. 8. Principal components of the (a) first and (b) second season-reliant EOF mode of the A–AM system during the pre-1979 and post-1979 epochs.

(−0.49) leading ENSO by 1 yr, which suggests that the first mode in the first epoch leads to a cooling phase of ENSO 1 yr later. This supports the fact that the first mode in the pre-1979 epoch has a stronger biennial tendency.

The eastward propagation of the zonal wind anomalies was more systematic in the pre-1979 epoch than in the recent epoch (Figs. 5b and 5c), suggesting that the biennial tendency is accompanied by a more evident eastward migration of zonal wind anomalies. We observe also that the eastward relocation of the zonal wind anomaly is slower in the recent epoch, as evidenced by the steeper tilt of the zero line in the zonal wind anomaly (Figs. 5b and 5c), which is consistent with the prolonged periodicity of A–AM variability during the recent decades.

Important interdecadal changes are seen from the seasonally evolving spatial patterns of the first S-EOF mode during the two epochs (Fig. 9a). The common features discussed in section 3a remain valid for each epoch; especially notable is the remarkable similarity in the anomalous circulation during SON(0). However, in the mature phase, DJF(0/1), of the recent epoch, the WNP anomalous anticyclone and the associated easterly anomalies from Indonesia to the equatorial Indian Ocean are strengthened, indicating a more robust ENSO–WNP relationship. The enhanced descent over Indonesia confirms the enhanced connection between ENSO and the drying condition over Indonesia, as suggested by Chang et al. (2004).

More prominent epochal changes are found in El Niño's developing phase during JJA(0) and decaying phase of MAM(1) to JJA(1). The Indian summer monsoon was weaker prior to the late 1970s, as evidenced by the anomalous subsidence over India and the reduced southwest monsoon over the Arabian Sea; in contrast, after the late 1970s, the Bay of Bengal exhibits ascent, and the southwest monsoon increases over the Arabian Sea. This change is related to the fact that in the recent epoch, the cyclonic anomaly over the WNP, the anticyclonic ridge extending from the Maritime Continent to the Arabian Sea, and the associated westerly monsoon flows from the northern Arabian Sea to the Philippine Sea have all become enhanced during the developing phase of El Niño. As such, the relationship between ENSO SST anomalies and the rainfall anomalies in the WNP and Southeast Asian monsoon region have become enhanced (Fig. 9a). During the decaying phase of El Niño, from MAM(1) to JJA(1), both the WNP anticyclonic anomalies and the SIO anticyclonic anomalies lasted longer in the post-1979 ep-

TABLE 2. As in Table 1 except that the correlation coefficients are calculated for the pre-1979 (1956–79) and post-1979 (1980–2003) epochs, respectively.

	S-EOF1(0)		S-EOF2(0)	
	56–79	80–03	56–79	80–03
Niño-3.4 SSTA(0)	**0.82**	**0.89**	0.35	0.06
Niño-3.4 SSTA(+1)	**−0.49**	−0.21	0.05	**0.82**

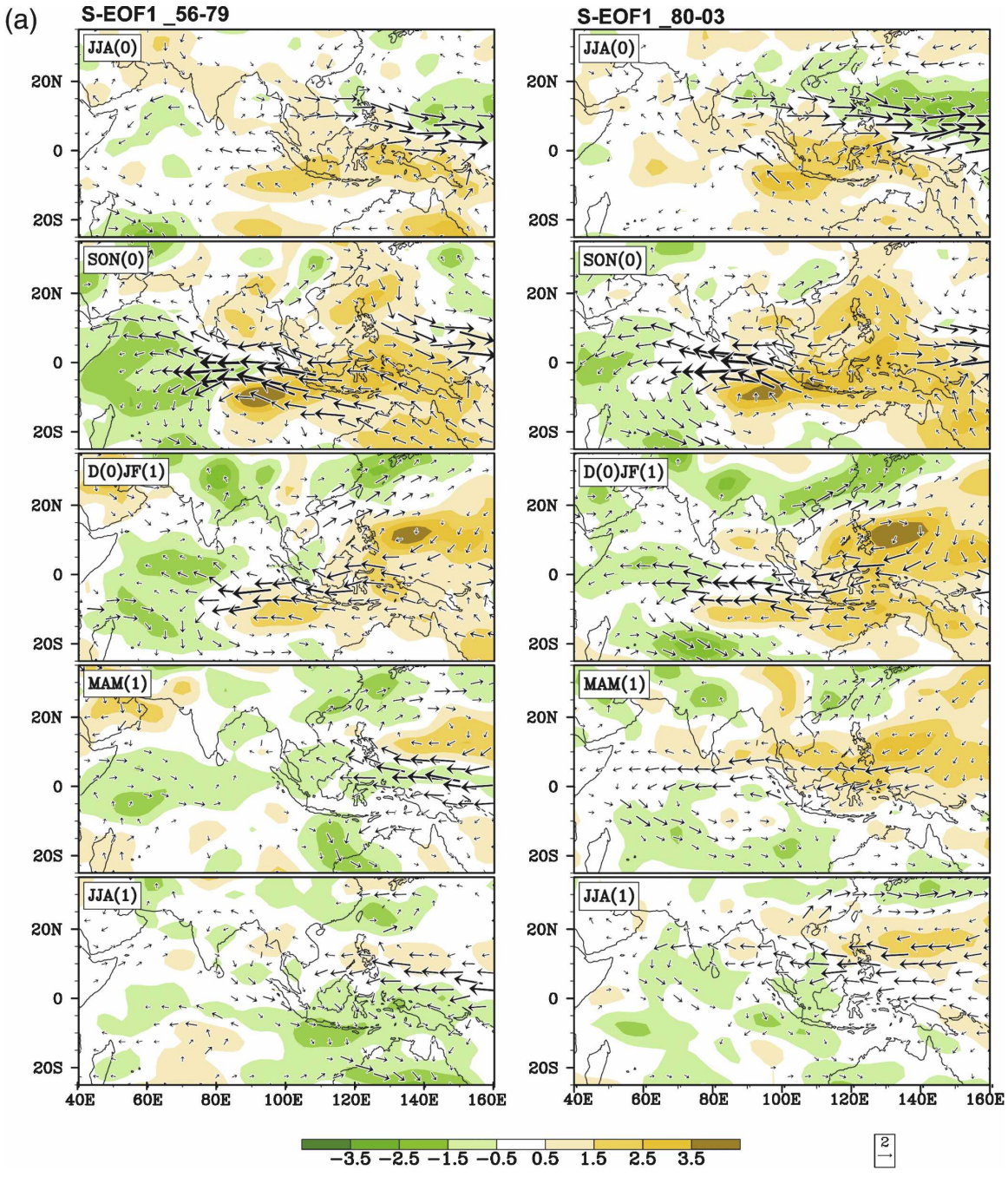

FIG. 9. (a) As in Fig. 3a but for the pre-1979 and post-1979 epochs. (b) Seasonal mean SST anomalies regressed upon the time coefficients of the first dominant S-EOF mode for the two epochs.

och. Thus, the East Asian meiyu front received increased precipitation in the summer after the maturity of an El Niño. This "prolonged" ENSO impact on the EA monsoon via the WNP anticyclone (Wang et al. 2000) has been reinforced since the late 1970s. In summary, while the Indian monsoon–ENSO relationship has weakened, the EA–WNP monsoon–ENSO relationship has enhanced in both the developing and decaying phases of ENSO.

The differences in the spatial patterns shown in Fig. 9a are closely associated with the most striking differences in the SST anomaly field (Fig. 9b). In the developing phase, the Niño-3.4 warming and the western Indian Ocean warming are stronger in the pre-1979 ep-

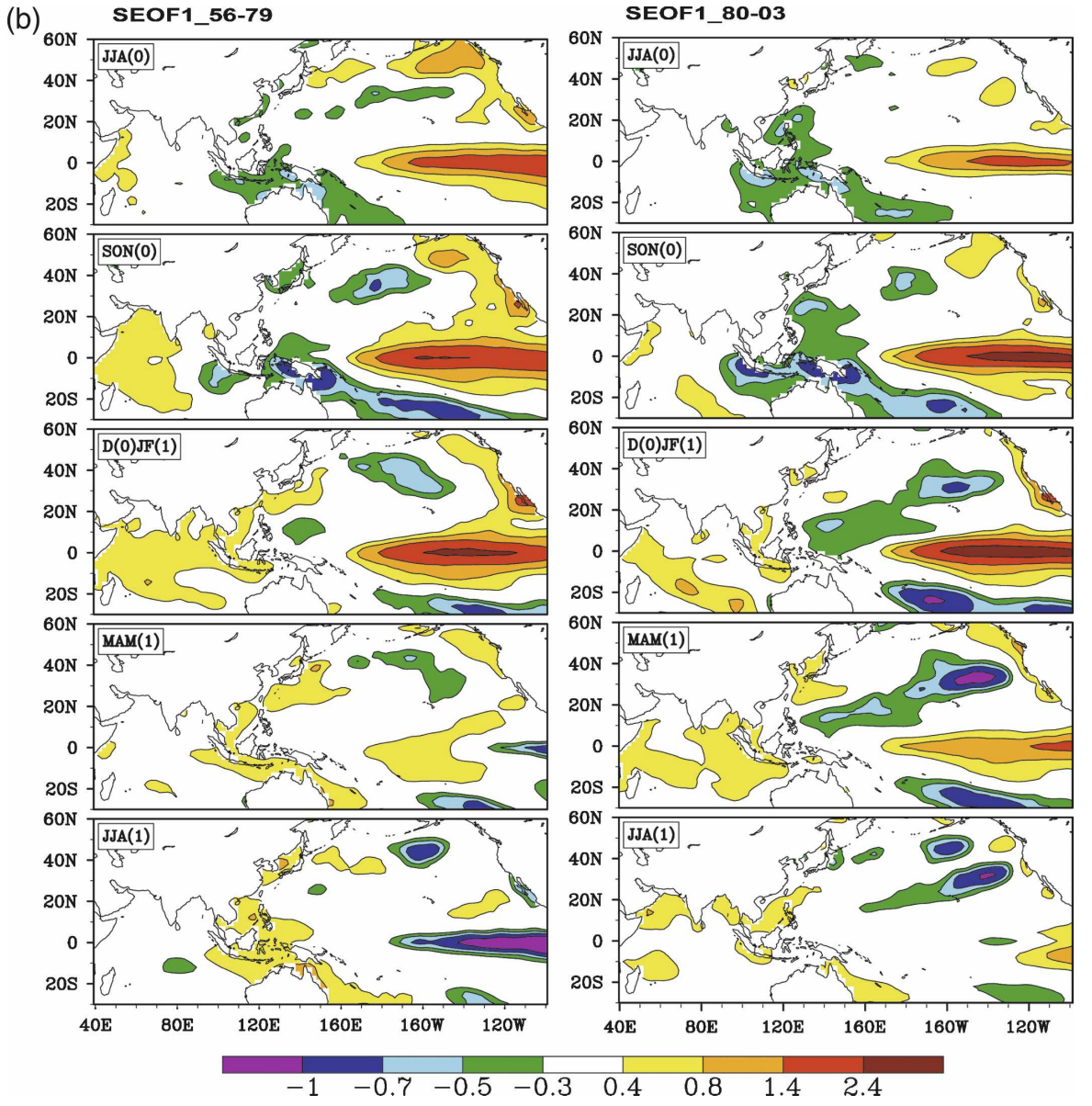

FIG. 9. (*Continued*)

och. This favors a weaker Indian summer monsoon rainfall. During the mature phase, DJF(0/1), the SST anomalies in the Pacific are stronger in the recent epoch, causing stronger abnormal Walker circulation. In the decaying phases, MAM(1) and JJA(1), the pre-1979 El Niño events dissipated more quickly: a cooling started from the eastern Pacific in MAM(1) and then progressed westward into the central equatorial Pacific in JJA(1). However, after the late 1970s, the warming in the equatorial eastern Pacific has persisted to MAM(1) and even in JJA(1). This encourages an enhanced delayed relationship between the EA–WNP monsoon and ENSO.

b. Changes in the second mode

Similar to the first mode, the second mode has also increased in fractional variance from 11.7% in the pre-1979 epoch to 15.7% in the recent epoch (Fig. 8b). The spectral peak at about 5 yr has become more significant in the recent epoch (figure not shown). The relationship between ENSO and the second mode has changed remarkably. Table 2 indicates that during the post-1979 epoch, the second S-EOF mode has a maximum correlation coefficient (about 0.82) leading El Niño by one year, suggesting that it may provide a precursory signal for ENSO onset. However, during the pre-1979 epoch,

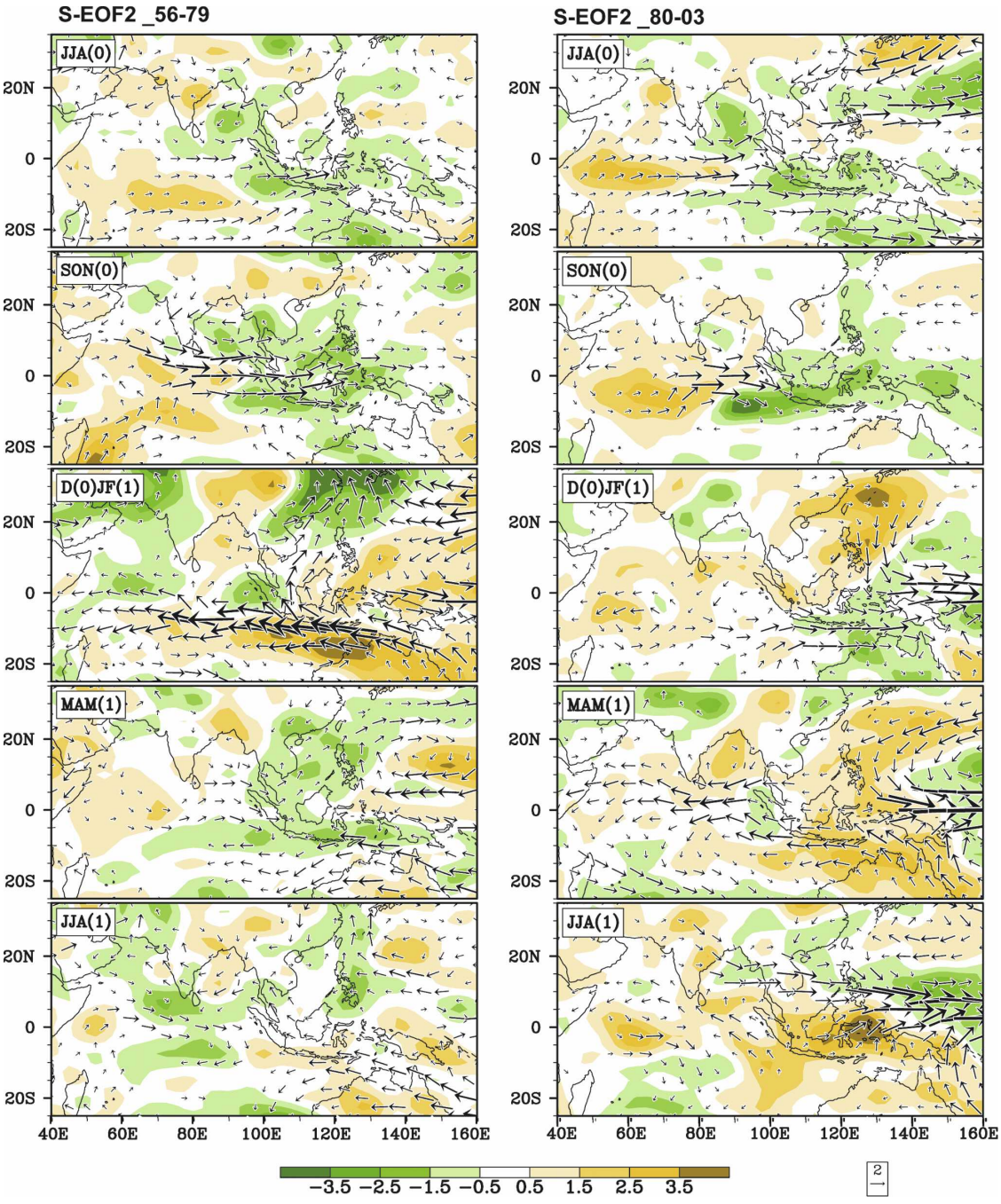

FIG. 10. As in Fig. 9a but for the second S-EOF mode.

the second leading mode does not lead ENSO at all but instead tends to be concurrent with ENSO turnaround (the correlation coefficient is about 0.35).

Circulation anomalies associated with the second S-EOF mode over the A–AM region also undergo significant interdecadal change (Fig. 10). In the post-1979 epoch, about a year prior to the El Niño mature phase, westerly anomalies are well established over the equatorial western Pacific, and these anomalies continuously grow during the next two seasons, leading to the development of an El Niño episode (Fig. 10). These westerly anomalies are associated with the Philippine Sea cyclonic anomaly. This feature has been pointed out earlier in Wang (1995a), who examined the interdecadal change in ENSO's onset. However, during the pre-1979 epoch, such a precursor signal does not exist;

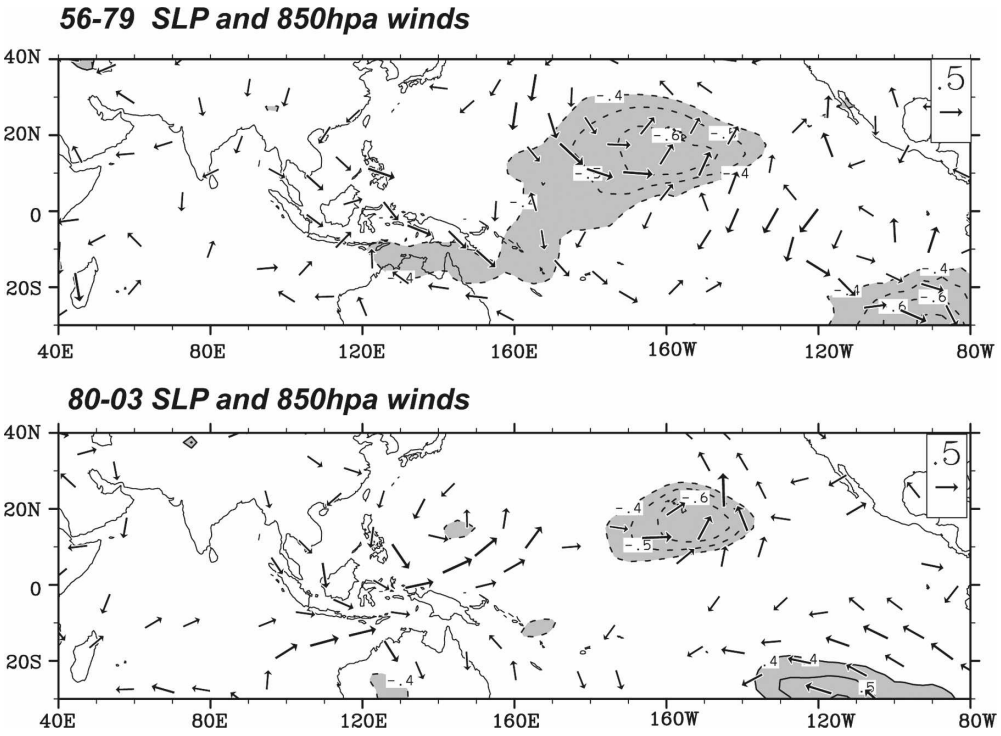

FIG. 11. Statistically significant 850-hPa winds (vectors, m s^{-1}) and sea level pressure (contours, hPa) 12 months prior to the ENSO mature phase for the pre-1979 and post-1979 epochs. These anomalies were derived from a 12-month lead correlation with reference to the DJF SST anomalies in the Niño-3.4 region.

instead, anomalous subsidence over the Australian summer monsoon (implying a weak Australian summer monsoon) leads El Niño (Fig. 10).

Changes in the second mode implies that in the transition phase of ENSO, namely, about 12 months before the mature phase of an El Niño episode, the ENSO precursory conditions have been changed since the late 1970s. As shown in Fig. 11, one year prior to maturity of El Niño events, the Philippine Sea cyclonic anomaly and associated equatorial westerly anomaly north of New Guinea are a feature for the post-1979 epoch only. Of interest is that in the pre-1979 epoch weakening of North Pacific subtropical high (the cyclonic anomaly) is a notable precursor, but this feature has become less prominent in the post-1979 epoch when the Philippine Sea cyclonic anomaly has become prominent. In a previous study, Wang (1995b) noticed a similar El Niño precursor using the Comprehensive Atmosphere–Ocean Dataset.

c. *Changes in the regional monsoon and ENSO relationship*

Results in Fig. 9 confirm that after the late 1970s, the Indian summer monsoon and ENSO relationship has broken down (Kumar et al. 1999). However, the results also reveal that the relationships between ENSO and the western North Pacific, East Asian, and Indonesian monsoons have become enhanced. To confirm this assertion, we have further examined relationship between the Niño-3.4 SST anomaly and three regional monsoon indices for the two epochs (Fig. 12).

The regional monsoon circulation indices were designed to measure the interannual variability of the western North Pacific summer monsoon (WNPSM; Wang and Fan 1999) and the ISM (Wang et al. 2001). They are defined by the meridional shear vorticity of the 850-hPa zonal wind anomaly (U850) as follows:

WNPSMI: U850(5°–15°N, 100°–130°E) minus U850(20°–30°N, 110°–140°E)

ISMI: U850(5°–15°N, 40°–80°E) minus U850(20°–30°N, 70°–90°E).

The meteorological meaning of these indices is discussed in details in Wang et al. (2001). In addition, a circulation index for the maritime continental region is defined by the 850-hPa westerly anomaly averaged over the region encompassed by 5°N–5°S, 100°–140°E.

The lead–lag correlations of the three regional monsoon indices with reference to the ENSO mature phase DJF(0/1) are shown in Fig. 12. We note that the significant correlation between the ISM and ENSO in the

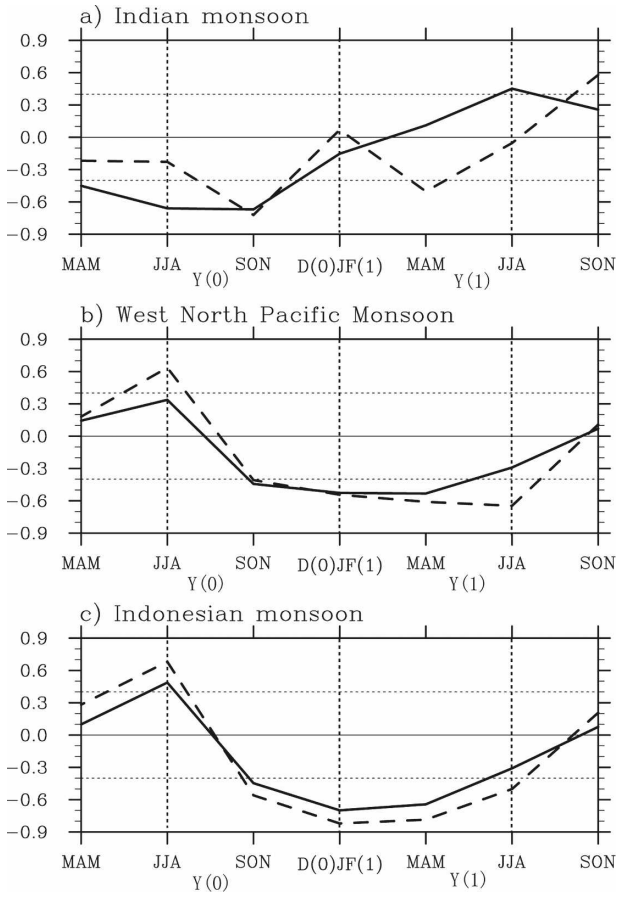

FIG. 12. Lead–lag correlation coefficients of the seasonal mean anomalies of three regional monsoon indices with reference to the DJF(0/1) Niño-3.4 SST anomalies for the pre-1979 (solid line) and post-1979 (dashed line) epochs, respectively. The notations (0) and (1) denote the developing and the decaying year of the El Niño event, respectively. The definitions for (a) Indian, (b) western North Pacific, and (c) Indonesian monsoon circulation indices are referred to in the text. The horizontal dotted lines show the 95% significant level.

1956–79 epoch has broken down after 1979 in both ENSO's developing year (year 0) and its decaying year (year 1), indicating a substantial weakening of the coupling between the ISM and ENSO (Fig. 12a). This result not only confirms the weakening anticorrelation in the developing phase of ENSO derived by using all Indian rainfall as an index (Kumar et al. 1999) but also reveals the weakening of the positive ISM–ENSO correlation in the decaying phase of ENSO. The latter is a new finding.

The weakening of the ISM–ENSO relationship in both the developing and decaying year implies that biennial oscillation of the ISM has become insignificant after 1979. It is interesting that the interdecadal change in ISM–ENSO correlation/anticorrelation depends strongly on season. The anticorrelation between ISM and ENSO remained in both epochs in SON(0), one season prior to the ENSO maturity. Further, the anticorrelation has become enhanced in MAM(1), one season after the mature phase of ENSO.

In sharp contrast to the weakening ISM–ENSO coupling, the relationship between the WNPSM and ENSO has strengthened considerably in both the ENSO developing year and the decaying year (Fig. 12b). In the 1956–79 epoch the WNPSM–ENSO correlation was not statistical significant in both the developing and decaying phases. But both the positive correlation in the developing phase and the negative correlation in the decaying phase have become statistically significant after 1979. The East Asian monsoon–ENSO relationship has also become reinforced after the late 1970s, because the East Asian subtropical monsoon is closely coupled with the WNPSM through the so-called Pacific–Japan pattern (Nitta 1987). The variance in U_{850} associated with the first mode in southeast China has increased in the northern summers of both ENSO's developing and decaying phases (figure not shown here). Since the late 1970s the equatorial Maritime Continent monsoon (5°N–5°S, 100°–140°E) and ENSO correlation has been strengthened throughout the year from the developing to decaying phase (Fig. 12c). The enhanced coupling between ENSO and the WNP–EA and Indonesian monsoons since 1980 has been overlooked in the past.

5. What gives rise to the interdecadal change in the first leading mode of variability?

To answer the question raised in the title of this section, we should first explain which factors determine the first leading mode of A–AM interannual variability.

a. Factors determining the first leading mode of variability

The remote El Niño/La Niña forcing is the chief factor that affects A–AM variability. However, A–AM anomalies are not solely forced by ENSO. As seen in Fig. 3, A–AM circulation anomalies are characterized by the SIO and WNP anomalous anticyclones, and their variations are not in phase with ENSO forcing. As shown in Fig. 4, the Niño-3.4 SST anomaly and the corresponding remote forcing from the eastern Pacific reach their maximum in the northern winter, DJF(0/1). However, the SIO anticyclone peaks one season earlier, while the WNP anticyclone reaches its maximum strength one season after the El Niño peak. The mismatch between Niño-3.4 SST and the evolution of the two major A–AM circulation anomalies suggests that El Niño alone cannot force these anomalies.

A widely held view in the literature considers the complementary SST anomalies in the Indo-Pacific warm pool to be additional sources of A–AM variability. In our view, this is far from a full story. The warm pool SST anomalies themselves are largely a result of anomalous monsoon forcing except in some limited regions. Thus, local SST anomalies cannot be regarded as a cause of the monsoon variation. We advocate that the local monsoon–warm ocean interaction is one of the fundamental causes responsible for the monsoon anomalies (e.g., Wang et al. 2000, 2003; Wu and Kirtman 2005; Wu et al. 2006).

Three major monsoon–ocean interaction mechanisms have been proposed in the literature. The growth of the Indian Ocean dipole anomaly is regarded as resulting from a positive feedback between equatorial zonal winds and the zonal SST gradient via changing oceanic thermocline depth and excitation of the equatorial oceanic Kelvin waves (Webster et al. 1999; Saji et al. 1999). This mechanism is an application of the Bjerknes (1969) theory to the equatorial Indian Ocean.

The second mechanism emphasizes the feedback between the off-equatorial convectively coupled Rossby waves and east–west dipole SST anomalies (Rossby wave–SST dipole feedback) originally proposed by Wang et al. (2000) to explain why ENSO has a delayed impact on the East Asian summer monsoon two seasons after its maturity. A key factor that conveys the prolonged ENSO impact on the East Asian summer monsoon is the persistence of the WNP anomalous anticyclone during the decaying phase of El Niño. The reason that explains why the WNP AC can maintain itself against the decay of the ENSO forcing is attributed to Rossby wave–SST dipole interaction in the warm pool. Over the WNP, due to the presence of the mean northeasterly trade winds and winter monsoon, the ocean to the east of the WNP AC cools due to increased total wind speed, which induces excessive evaporation and entrainment cooling. The cooling, in turn, suppresses atmospheric convection and reduces latent heating, which excites westward-propagating, descending Rossby waves that reinforce the AC anomaly. This hypothesis has been demonstrated by numerical experiments using an atmospheric general circulation model and its coupled version (Lau et al. 2004).

The Rossby wave–SST dipole feedback mechanism was also used to explain why the SIO AC and Indian Ocean dipole rapidly intensify from summer to fall and why the cooling near Sumatra disappears rapidly after November, as well as why the SST anomalies in the southwest Indian Ocean can continue after the mature phase of El Niño (Wang et al. 2003). During the development of El Niño, for instance, the boreal summer monsoon flows dominate in the Indian Ocean. The SIO AC and IOD have a positive feedback because the southeasterly anomaly to the east of the SIO AC enhances the cold SST anomalies by increasing wind speed along the coast of Sumatra and the equatorial Indian Ocean, thereby favoring coastal and equatorial upwelling and evaporation–entrainment cooling. The cooling that occurs off the coast of Sumatra in turn suppresses local convective heating, which excites the descent atmospheric Rossby waves that reinforce the SIO AC anomaly on their decaying journey to the west. Therefore, the rapid amplification of the SIO anticyclonic anomaly and the maintenance of the WNP anticyclonic anomaly involve a common Rossby wave–SST dipole coupling, although the role of oceanic dynamics in causing SST variations in the two basins are different. Of particular note is that the positive feedback between the SIO anticyclone and the IOD SST anomaly depends on boreal summer monsoon flows. Once the summer monsoon changes to the winter monsoon after November, the background flows reverse direction north of the SIO convergence zone (along 10°–15°S), which switches the positive feedback to a negative one. Therefore, the cold pole off Sumatra decays rapidly and sometimes transforms to a weak warming (shown by the contours in Fig. 3b). This explains why the southeast Indian Ocean cooling reaches a maximum intensity in the boreal fall (Saji et al. 1999) and why the warming in the subtropical southwest Indian Ocean remains after the fall, leading to the transition from a dipole mode to a basinwide warming mode.

The third mechanism is a monsoonal negative feedback that tends to offset the effects of remote forcing. This negative feedback can be realized through either surface heat flux exchange or through oceanic Ekman layer heat transport. By comparing an atmospheric general circulation model simulation and its coupled model simulation, Lau and Nath (2000) found that the El Niño–induced reduction of Indian monsoon precipitation favors warming in the northern Indian Ocean (due to reduced evaporation cooling and increased solar radiation), which in turn enhances the Indian monsoon by converging water vapor into the monsoon trough, thereby offsetting the effects of El Niño. Webster et al. (2002) and Loschnigg et al. (2003) proposed that a strong monsoon, which is related to stronger-than-normal low-level monsoon flows, drives an enhanced southward Ekman heat transport. This tendency produces a meridional temperature gradient that tends to weaken the monsoon. This negative feedback may lead to monsoon anomalies that have a mathematically opposite sign in the following year, thus regulating the monsoon's interannual variability and introducing a bi-

ennial component into the monsoon system (Meehl 1997).

In addition to the remote El Niño forcing and local monsoon–warm ocean interaction, an often overlooked factor is the role of the annual cycle. The annual cycle plays dual roles. First, the monsoon annual cycle controls the nature of the monsoon–ocean feedback. Second, the mean flows associated with the annual cycle can remarkably modify the atmospheric response to remote El Niño forcing, as shown by Wang et al. (2003).

b. What gives rise to interdecadal changes in the first leading mode of A–AM variability?

We argue that the changes in ENSO behavior, the changes in the strength of the local monsoon–warm pool ocean interaction, and the coupling between the Indian and Pacific Ocean are conceivable sources of the major modal' interdecadal changes.

After the late 1970s, the ENSO amplitude has increased and ENSO periodicity has become longer (e.g., Wang and Wang 1996; Gu and Philander 1997; An and Wang 2000). The interdecadal change in ENSO properties has been attributed to the interdecadal changes in the tropical Pacific mean state (Wang 1995a; Fedorov and Philander 2000; Wang and An 2002), which possibly result from changes in the North Pacific (Barnett et al. 1999) and/or South Pacific (Chang et al. 2001) or from stochastic forcing (Flügel and Chang 1999). Thus, the interdecadal change in ENSO can be largely independent from A–AM and can be regarded as one of the causes of interdecadal changes in the first mode of A–AM variability.

The increased ENSO amplitude since the late 1970s has reinforced the anomalous Walker circulation. This is confirmed by the enhanced correlation between Niño-3.4 SST anomalies and the equatorial Maritime Continent monsoon (5°N–5°S, 100°–140°E; shown in Fig. 12c). This may result in the increased fractional variance of the two major A–AM modes, as both are related to ENSO.

With the increased amplitude of ENSO in the recent epoch, the ENSO-induced local air–sea interaction in the Indian sector has also increased considerably. The increase in IOD amplitude is one example. The local air–sea interaction and IOD in the developing phase of ENSO tend to counteract the ENSO effects on the Indian monsoon (e.g., Lau and Nath 2000). Therefore, the local coupling might have caused a reduction in the ENSO–ISM relationship. Over the western North Pacific sector, the situation is the opposite. The WNPSM response to ENSO forcing has increased in accordance with ENSO's increasing strength, as it is a direct Rossby response to ENSO forcing in the developing phase of the ENSO. The strengthened ENSO induces stronger local air–sea interaction over the western North Pacific region during the mature phase, and therefore, the resultant WNP anticyclonic anomalies have become stronger since the late 1970s. This leads to a strengthened relationship between ENSO and the western North Pacific summer monsoon and East Asian summer monsoon during the summer of the ENSO decaying phase.

The ENSO has a significant biennial component before 1979, while the biennial tendency after 1979 is primarily associated with ENSO turnaround. This may partially explain changes in the dominant frequency of A–AM variation. In the recent epoch, all major ENSOs are accompanied by a strong IOD, and thus, the association of the biennial tendency with ENSO turnabout may be due to the influence of the IOD. During the pre-1979 epoch, the stronger biennial tendency of the A–AM first mode is consistent with the stronger biennial component of ENSO. Further, the positive IOD events (1961, 1967, and 1972) and negative IOD events (1960, 1964, and 1975) also contributed to the biennial tendency during the first epoch (Fig. 8a).

6. Conclusions and discussion

Using season-reliant EOF analysis, we found two statistically distinguishable modes of interannual variability in the A–AM system. The first mode exhibits a significant biennial tendency and concurs with ENSO turnaround from a warm to a cold phase; it essentially reflects the phenomenon of the tropical biennial oscillation (TBO) and provides a new perspective of the seasonally evolving spatiotemporal structure for TBO. As such, it may be used to define the TBO (at least in the A–AM domain).

The causes of the first leading mode has been attributed to 1) remote ENSO forcing, 2) local monsoon–oceanic warm pool interaction, and 3) the regulation of the powerful monsoon annual cycle (Wang et al. 2003). These processes are also essential for sustaining the TBO. Of note is that the first and second S-EOF modes of the Pacific–Indian Ocean SST represent the low-frequency (LF) and quasi-biennial (QB) component, respectively. On the other hand, the first and second A–AM S-EOF modes are QB and LF modes, respectively. This mismatch suggests that, while A–AM anomalies are influenced by ENSO, the intrinsic mechanisms within the A–AM system itself (such as monsoon–warm ocean interaction) play an important role in shaping its biennial tendency and modifying the response of the monsoon to ENSO. In contrast to the conventional viewpoint that warm pool SST anomalies

are a source of A–AM variability, we believe it is the monsoon–oceanic warm pool interaction, rather than the warm pool SST itself, that should be regarded as a cause. The monsoon–warm pool interaction is characterized by a positive feedback between moist atmospheric Rossby waves and the underlying SST dipole anomalies. In addition, the seasonal march of monsoon flows also plays an important "hidden" role by determining the nature of the monsoon–ocean interaction and by modifying the monsoon response to remote El Niño forcing.

The seasonal evolution of the first leading mode is characterized by a pair of anomalous anticyclones (ACs) over the south Indian Ocean (SIO) and western North Pacific (WNP), which peak, respectively, in the boreal fall of the El Niño development phase and the subsequent spring. The principal component of the second S-EOF mode has a spectral peak at the 5-yr point and leads Niño-3.4 SST anomalies by about one year, providing a precursor for El Niño/La Niña development.

The major modes of A–AM variations have significantly changed since the late 1970s. These changes include the following attributes:

- The fractional variance accounted for by the first and second S-EOF modes, which both reflect the ENSO–monsoon connection, has increased from 35.9% to 46.9% since the late 1970s (Fig. 8).
- In the pre-1979 epoch, the quasi-biennial oscillation and eastward migration of the equatorial zonal wind anomalies are more evident than in the post-1979 epoch (Figs. 5 and 8).
- Since the late 1970s, the South Asian monsoon westerly, extending from the northern Arabian Sea to the Philippine Sea, has become significantly enhanced during the El Niño developing phase, which in turn weakens the anticorrelation between the Indian summer monsoon and ENSO but strengthens the positive correlation between ENSO and the western North Pacific and Southeast Asian monsoon rainfall (Fig. 9a). During the mature phase of ENSO, the WNP anomalous anticyclone and the associated easterly anomalies have also strengthened in the recent epoch, resulting in an enhanced ENSO–Indonesian monsoon relationship (Fig. 12c).
- In the post-1979 epoch, the WNP anticyclonic anomalies have lasted longer in the decay phase of ENSO; thus, in the summer after the maturity of an El Niño occurrence, the WNP and East Asian summer monsoon has strengthened its relationship with ENSO (Fig. 12).
- Only during the post-1979 epoch, the second S-EOF mode provides a useful precursory signal for ENSO warming. Such a precursor signal does not exist in the pre-1979 epoch (Figs. 10, 11).

The above results together suggest that the overall coupling between the A–AM system and ENSO has been enhanced since the late 1970s because positive correlations between ENSO and the western North Pacific, East Asian, and Indonesian monsoons have all become enhanced during the developing, maturity, and decaying phases of ENSO, regardless of the weakening of the Indian monsoon–ENSO anticorrelation during the ENSO developing phase (Fig. 12). The second S-EOF mode represents a possible influence of the A–AM on ENSO, which is evident only in the recent epoch, also suggesting the strengthening coupling between A–AM system and ENSO.

Why have the major modes of A–AM variability changed since the late 1970s? The interdecadal change is ascribed to increased ENSO forcing and A–AM feedback to ENSO. Figure 13 outlines our major points of this explanation. The enhanced ENSO variability in the recent epoch has increased the strength of the monsoon–warm pool interaction and the Indian Ocean dipole SST anomalies, which has strengthened the summer westerly monsoon across South Asia, thus weakening the negative linkage between the Indian summer monsoon rainfall and the eastern Pacific SST anomaly. Meanwhile, the amplified ENSO forcing and the induced monsoon–ocean interaction have reinforced the impact of ENSO on the East Asian, western North Pacific, and Indonesian monsoons.

The interdecadal changes are detected by contrasting the two periods, 1956–late 1970s and late 1970s–2004 (roughly two 24-yr periods). Examining the results derived from an earlier period (1948–55) shows that the second S-EOF also represents the precursor of El Niño events, suggesting that the interdecadal changes detected here might exist in the pre-1950s period and are not necessarily unique to the recent epoch.

This study has established an objective measure for assessing broad-scale Asian–Australian monsoon interannual variability. The two major modes provide useful metrics for gauging A–AM system variability in atmospheric general circulation models and in coupled climate models. The hypothesis made here concerning the causes of the major modes and their interdecadal variation emphasizes the combined effects of remote ENSO forcing and the local monsoon–oceanic warm pool interaction. This hypothesis needs further validation through numerical experiments with coupled atmosphere–ocean models that can produce reasonably realistic climatology and interannual anomalies. Further

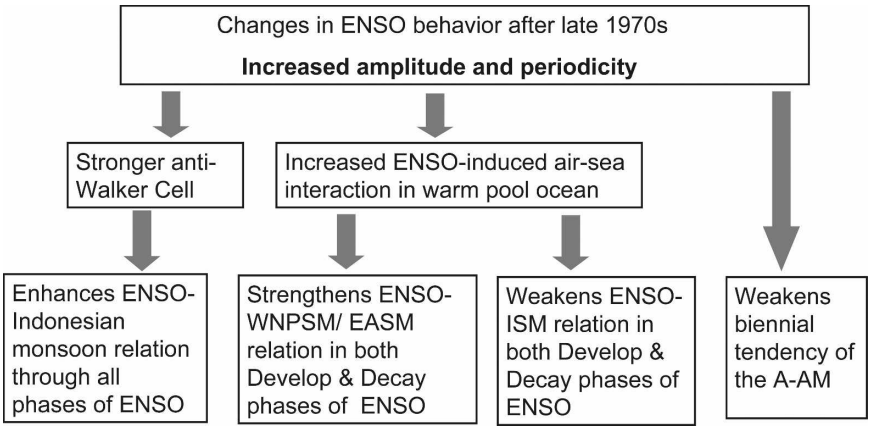

FIG. 13. A schematic diagram is presented to illustrate how the A–AM responds to the increased ENSO forcing after late 1970s.

diagnosis of the Intergovernmental Panel on Climate Change (IPCC) Fourth Assessment Report (AR4) simulations may not only validate the models but also shed light on the validity of the proposed mechanism. This effort is currently being undertaken, and the findings will be reported elsewhere.

Acknowledgments. The first two authors are supported by the Climate Dynamics Program of the National Science Foundation and the NOAA OGP through CLIVAR/Pacific Program. The International Pacific Research Center is in part sponsored by the Japan Agency for Marine-Earth Science and Technology.

REFERENCES

An, S.-I., and B. Wang, 2000: Interdecadal change of the structure of the ENSO mode and its impact on the ENSO frequency. *J. Climate,* **13,** 2044–2055.

Barnett, T. P., D. W. Pierce, M. Latif, D. Dommenget, and R. Saravanan, 1999: Interdecadal interactions between the tropics and midlatitudes in the Pacific basin. *Geophys. Res. Lett.,* **26,** 615–618.

Bjerknes, J., 1969: Atmospheric teleconnections from the equatorial Pacific. *Mon. Wea. Rev.,* **97,** 163–172.

Chang, C.-P., Z. Wang, J. Ju, and T. Li, 2004: On the relationship between western maritime continent monsoon rainfall and ENSO during northern winter. *J. Climate,* **17,** 665–672.

Chang, P., B. S. Giese, L. Ji, H. F. Seider, and F. Wang, 2001: Decadal change in the south tropical Pacific in a global assimilation analysis. *Geophys. Res. Lett.,* **28,** 3461–3464.

Chen, M., P. Xie, J. E. Janowiak, and P. A. Arkin, 2002: Global land precipitation: A 50-yr monthly analysis based on gauge observations. *J. Hydrometeor.,* **3,** 249–266.

Chen, T.-C., and J.-H. Yoon, 2000: Interannual variation in Indochina summer monsoon rainfall: Possible mechanism. *J. Climate,* **13,** 1979–1986.

Fedorov, A. V., and S. G. Philander, 2000: Is El Niño changing? *Science,* **288,** 1997–2002.

Flügel, M., and P. Chang, 1999: Stochastically induced climate shift of El Niño–Southern Oscillation. *Geophys. Res. Lett.,* **26,** 2473–2476.

Graham, N. E., 1994: Decadal-scale climate variability in the tropical and North Pacific during the 1970s and 1980s: Observations and model results. *Climate Dyn.,* **10,** 135–162.

Gu, D., and S. G. H. Philander, 1997: Interdecadal climate fluctuations that depend on exchanges between the tropics and extratropics. *Science,* **275,** 805–807.

Hamada, J. I., M. D. Yamanaka, J. Matsumoto, S. Fukao, P. A. Winarso, and T. Sribimawati, 2002: Spatial and temporal variations of the rainy season over Indonesia and their link to ENSO. *J. Meteor. Soc. Japan,* **80,** 285–310.

Huang, R., and Y. Wu, 1989: The influence of ENSO on the summer climate change in China and its mechanism. *Adv. Atmos. Sci.,* **6,** 21–32.

Janowiak, J. E., 1988: An investigation of interannual rainfall variability in Africa. *J. Climate,* **1,** 240–255.

Kalnay, E., and Coauthors, 1996: The NCEP/NCAR 40-Year Reanalysis Project. *Bull. Amer. Meteor. Soc.,* **77,** 437–471.

Kim, K.-M., and K.-M. Lau, 2001: Dynamics of monsoon-induced biennial variability in ENSO. *Geophys. Res. Lett.,* **28,** 315–318.

Kumar, K. K., B. Rajagopalan, and M. A. Cane, 1999: On the weakening relationship between the Indian monsoon and ENSO. *Science,* **284,** 2156–2159.

Lau, K.-M., and P. J. Sheu, 1988: Annual cycle, quasi-biennial oscillation, and Southern Oscillation in global precipitation. *J. Geophys. Res.,* **93,** 10 945–10 988.

——, and H. T. Wu, 2001: Principal modes of rainfall–SST variability of the Asian summer monsoon: A reassessment of the monsoon–ENSO relationship. *J. Climate,* **14,** 2880–2895.

Lau, N.-C., and M. J. Nath, 2000: Impact of ENSO on the variability of the Asian–Australian monsoons as simulated in GCM experiments. *J. Climate,* **13,** 4287–4309.

——, and B. Wang, 2005: Monsoon–ENSO interactions. *The Global Monsoon System: Research and Forecast,* WMO Tech. Doc. 1266 and TMRP Rep. 70, 299–309.

——, M. J. Nath, and H. Wang, 2004: Simulations by a GFDL GCM of ENSO-related variability of the coupled atmosphere–ocean system in the East Asian Monsoon region. *East*

Asian Monsoon, C.-P. Chang, Ed., World Scientific Series on Meteorology of East Asia, Vol. 2, World Scientific, 271–300.

Loschnigg, J., G. A. Meehl, P. J. Webster, J. M. Arblaster, and G. P. Compo, 2003: The Asian monsoon, the tropospheric biennial oscillation, and the Indian Ocean zonal mode in the NCAR CSM. *J. Climate,* **16,** 1617–1642.

Meehl, G. A., 1987: The annual cycle and interannual variability in the tropical Pacific and Indian Ocean regions. *Mon. Wea. Rev.,* **115,** 27–50.

——, 1997: The South Asian monsoon and the tropospheric biennial oscillation. *J. Climate,* **10,** 1921–1943.

——, and J. Arblaster, 2002: The troposphere biennial oscillation and Asian–Australian monsoon rainfall. *J. Climate,* **15,** 722–744.

Mooley, D. A., and B. Parthasarathy, 1984: Fluctuations in all-India summer monsoon rainfall during 1871–1978. *Climatic Change,* **6,** 287–301.

Navarra, A., M. N. Ward, and K. Miyakoda, 1999: Tropical-wide teleconnection and oscillation. I: Teleconnection indices and type I/type II states. *Quart. J. Roy. Meteor. Soc.,* **125,** 2909–2935.

Nitta, T., 1987: Convective activities in the tropical western Pacific and their impact on the Northern Hemisphere summer circulation. *J. Meteor. Soc. Japan,* **65,** 373–390.

——, and S. Yamada, 1989: Recent warming of tropical sea surface temperature and its relationship to the Northern Hemisphere circulation. *J. Meteor. Soc. Japan,* **67,** 375–383.

North, G. R., T. L. Bell, R. F. Cahalan, and F. J. Moeng, 1982: Sampling errors in the estimation of empirical orthogonal functions. *Mon. Wea. Rev.,* **110,** 699–706.

Okoola, R. E., 1999: A diagnostic study of the eastern Africa monsoon circulation during the Northern Hemisphere spring season. *Int. J. Climatol.,* **19,** 143–168.

Ropelewski, C. F., M. S. Halpert, and X. Wang, 1992: Observed tropospheric biennial variability and its relationship to the Southern Oscillation. *J. Climate,* **5,** 594–614.

Saji, N. H., B. N. Goswami, P. N. Vinayachandran, and T. Yamagata, 1999: A dipole mode in the tropical Indian Ocean. *Nature,* **401,** 360–363.

Shukla, J., 1987: Interannual variability of monsoons. *Monsoons,* J. S. Fein and P. L. Stephens, Eds., John Wiley and Sons, 399–463.

Smith, T. M., and R. W. Reynolds, 2004: Improved extended reconstruction of SST (1854–1997). *J. Climate,* **17,** 2466–2477.

Trenberth, K. E., and J. W. Hurrell, 1994: Decadal atmosphere–ocean variations in the Pacific. *Climate Dyn.,* **9,** 303–319.

Uppala, S. M., and Coauthors, 2005: The ERA-40 Re-Analysis. *Quart. J. Roy. Meteor. Soc.,* **131,** 2961–3012.

Wang, B., 1995a: Interdecadal changes in El Niño onset in the last four decades. *J. Climate,* **8,** 267–285.

——, 1995b: Transition from a cold to a warm state of the El Niño–Southern Oscillation cycle. *Meteor. Atmos. Phys.,* **56,** 17–32.

——, and Y. Wang, 1996: Temporal structure of the Southern Oscillation as revealed by waveform and wavelet analysis. *J. Climate,* **9,** 1586–1598.

——, and Z. Fan, 1999: Choice of south Asian summer monsoon indices. *Bull. Amer. Meteor. Soc.,* **80,** 629–638.

——, and S.-I. An, 2001: Why the properties of El Niño changed in the late 1970s. *Geophys. Res. Lett.,* **28,** 3709–3712.

——, and ——, 2002: A mechanism for decadal changes of ENSO behavior: Roles of background wind changes. *Climate Dyn.,* **18,** 475–486.

——, and Q. Zhang, 2002: Pacific–east Asian teleconnection. Part II: How the Philippine Sea anomalous anticyclone is established during El Niño development. *J. Climate,* **15,** 3252–3265.

——, and S.-I. An, 2005: A method for detecting season-dependent modes of climate variability: S-EOF analysis. *Geophys. Res. Lett.,* **32,** L15710, doi:10.1029/2005GL022709.

——, R. Wu, and X. Fu, 2000: Pacific–East Asian teleconnection: How does ENSO affect East Asian climate? *J. Climate,* **13,** 1517–1536.

——, ——, and K.-M. Lau, 2001: Interannual variability of the Asian summer monsoon: Contrasts between the Indian and the western North Pacific–East Asian monsoons. *J. Climate,* **14,** 4073–4090.

——, ——, and T. Li, 2003: Atmosphere–warm ocean interaction and its impacts on Asian–Australian monsoon variation. *J. Climate,* **16,** 1195–1211.

Webster, P. J., 2006: The coupled monsoon system. *The Asian Monsoon,* B. Wang, Ed., Springer Praxis, 3–66.

——, and S. Yang, 1992: Monsoon and ENSO: Selectively interactive systems. *Quart. J. Roy. Meteor. Soc.,* **118,** 877–926.

——, A. M. Moore, J. P. Loschnigg, and R. R. Leben, 1999: Coupled ocean–atmosphere dynamics in the Indian Ocean during 1997–98. *Nature,* **401,** 356–360.

——, C. Clark, G. Cherikova, J. Fasullo, W. Han, J. Loschnigg, and K. Sahami, 2002: The monsoon as a self-regulating coupled ocean–atmosphere system. *Meteorology at the Millennium,* R. P. Pearce, Ed., Academic Press, 198–219.

Wu, R., and B. Wang, 2000: Interannual variability of summer monsoon onset over the western North Pacific and the underlying processes. *J. Climate,* **13,** 2483–2501.

——, and ——, 2002: A contrast of the East Asian summer monsoon–ENSO relationship between 1962–77 and 1978–93. *J. Climate,* **15,** 3266–3279.

——, and B. P. Kirtman, 2005: Role of Indian and Pacific Ocean air–sea coupling in tropical atmospheric variability. *Climate Dyn.,* **25,** 155–170.

——, ——, and K. Pegion, 2006: Local air–sea relationship in observations and model simulation. *J. Climate,* **19,** 4914–4932.

Yang, S., and K.-M. Lau, 2006: Interannual variability of the Asian monsoon. *The Asian Monsoon,* B. Wang, Ed., Springer Praxis, 259–293.

Yasunari, T., 1991: The monsoon year—A new concept of the climate year in the tropics. *Bull. Amer. Meteor. Soc.,* **72,** 1331–1338.

——, and R. Suppiah, 1988: Some problems on the interannual variability of Indonesian monsoon rainfall. *Tropical Rainfall Measurements,* J. S. Theon and N. Fugono, Eds., Deepak, 113–122.

Zhou, T.-J., and R.-C. Yu, 2005: Atmospheric water vapor transport associated with typical anomalous summer rainfall patterns in China. *J. Geophys. Res.,* **110,** D08104, doi:10.1029/2004JD005413.